Impedance spectroscopy of reduced monoclinic zirconia

Dominik Eder*[ab] and Reinhard Kramer[a]

Received 27th March 2006, Accepted 14th August 2006
First published as an Advance Article on the web 24th August 2006
DOI: 10.1039/b604396h

Zirconia doped with low-valent cations (*e.g.* Y^{3+} or Ca^{2+}) exhibits an exceptionally high ionic conductivity, making them ideal candidates for various electrochemical applications including solid oxide fuel cells (SOFC) and oxygen sensors. It is nevertheless important to study the undoped, monoclinic ZrO_2 as a model system to construct a comprehensive picture of the electrical behaviour. In pure zirconia a residual number of anion vacancies remains because of contaminants in the material as well as the thermodynamic disorder equilibrium, but electronic conduction may also contribute to the observed conductivity. Reduction of zirconia in hydrogen leads to the adsorption of hydrogen and to the formation of oxygen vacancies, with their concentration affected by various parameters (*e.g.* reduction temperature and time, surface area, and water vapour pressure). However, there is still little known about the reactivities of defect species and their effect on the ionic and electronic conduction. Thus, we applied electrochemical impedance spectroscopy to investigate the electric performance of pure monoclinic zirconia with different surface areas in both oxidizing and reducing atmospheres. A novel equivalent circuit model including parallel ionic and electronic conduction has previously been developed for titania and is used herein to decouple the conduction processes. The concentration of defects and their formation energies were measured using volumetric oxygen titration and temperature programmed oxidation/desorption.

Introduction

Oxide ceramics are gaining more widespread use as refractory structural and functional materials in a wide range of dielectric and electronic applications.[1] Zirconium dioxide (ZrO_2), especially when doped with Y_2O_3, CaO or MgO, combines its high ionic conductivity with a high mechanical and chemical resistance[2–5] and thus is currently considered the most promising material for use as a solid electrolyte in gas sensors (λ-probes[6–9]) and solid oxide fuel cells (SOFC) [10–12]. Within the last decade, zirconia based materials have also gained technological and scientific interest in the field of heterogeneous catalysis.[13–17] The use of zirconia and sulfated zirconia as a constituent in mixed oxides in catalysts has been discussed intensively.[18–20] Active sites on the surface of such species are most likely electronic or structural defects that lower the bonding strength of adsorbed molecules, thereby favouring subsequent reactions. Because of structural and chemical properties similar to titania, zirconia may behave like titania when it is used as a support for noble metal catalysts. Currently, there is much interest in undoped zirconia for its role in solid solutions (*e.g.* with CeO_2) and its influence on catalysis.[21,22]

Unlike stabilised tetragonal or cubic zirconia, undoped ZrO_2 with monoclinic equilibrium structure is not suitable for electrical applications, as it undergoes a 5–9% volume shrinkage due to the monoclinic-to-tetragonal phase transition at 1350 K.[23] Nevertheless, it is important to study the undoped, monoclinic ZrO_2 as a model system to obtain a comprehensive picture of the electrical behaviour. Furthermore, any data of electronic conduction obtained for the undoped monoclinic zirconia may also be valid for stabilised tetragonal or cubic zirconia (*e.g.* YSZ), thereby improving our understanding of the electrochemical processes in SOFC and gas sensors. Since the working temperatures of catalysts generally remain well below temperatures needed for the monoclinic-to-tetragonal phase transition, the study of undoped monoclinic zirconia is of purely catalytic interest as well.

Zirconia is a stable oxide that tends to lose surface oxygen only after thermal treatment under high vacuum above 973 K.[2,24] Nevertheless, theoretical studies have predicted the presence of defect sites (anion vacancies) at significantly lower temperatures when zirconia is exposed to a reducing atmosphere.[25–30] FTIR and EPR studies focused on the chemisorption of CO and H_2/O_2 on pure zirconia and suggested the formation of oxygen deficient surface sites.[24,30–33] Previously, we were the first to verify the formation of oxygen vacancies and to measure their quantity in hydrogen treated monoclinic zirconia using volumetric oxygen titration.[34] Based on FTIR and EPR observations[32,35] we postulated the formation of a Zr^{3+}/e^- pair similar to that of oxygen vacancies in TiO_2.[36,37]

When zirconia is treated in hydrogen at temperatures below 873 K, surface oxygen vacancies are formed with an activation energy of 20 kJ mol^{-1} (0.22 eV), whereas the vacancies formed

[a] *Institut für Physikalische Chemie, Universität Innsbruck, Innrain 52a, 6020 Innsbruck, Austria. E-mail: reinhard.kramer@uibk.ac.at; Fax: +43 512 507 2925; Tel: +43 512 507 5057*
[b] *Department of Materials Science and Metallurgy, University of Cambridge, New Museums Site, Pembroke Street, Cambridge, UK CB2 3QZ. E-mail: de235@cam.ac.uk; Fax: +44 1223 335637; Tel: +44 1223 334335*

at higher temperatures need significantly higher activation energies of 120 kJ mol^{-1} (1.25 eV). Presumably, this higher activation energy originates from the diffusion of oxygen vacancies into the bulk of zirconia. The additional energy for oxygen diffusion of 1 eV was also measured in zirconia by tracer diffusion and impedance spectroscopy studies.[38,39]

The deviation from stoichiometry also affects the electrical behaviour of semi-conducting oxides like CeO_{2-x}.[5,40–42] or TiO_{2-x}.[36,43,44] Most studies of zirconia have been carried out on doped and stabilised zirconia samples, where the conductivity can be exclusively attributed to high ionic conductivity due to oxygen vacancies formed extrinsically by doping with low-valent cations.[4,5,45] However, hydrogen treatment can cause an additional conduction mechanism as described by Levy *et al*., who proposed a model for the electrical conductivity of electrochemically reduced stabilised zirconia with two different conduction processes (ionic and electronic) depending on the deviation from stoichiometry.[46] In a previous paper, we developed an alternative conduction model for substoichiometric titania using electrochemical impedance spectroscopy.[47]

Some authors reported higher electrical conductivities in zirconia at grain boundaries.[5,48–50] This raises the question whether the introduction of interfaces by nanostructurisation will contribute to a further enhancement of the electrical conductivity. However, until now undoped monoclinic zirconia has been rarely discussed.

Therefore, the aim of this work was to study the electric properties of undoped monoclinic zirconia in oxidizing and reducing atmospheres under various conditions including surface area, reduction temperature and oxygen partial pressure. This was done with electrochemical impedance spectroscopy on nanocrystalline as well as on coarse-grained zirconia samples with controlled stoichiometry.

Experimental

Materials

The zirconium(IV) oxide used in this work was prepared by low temperature drying of a solution of zirconia-aquat (a suspension of 20% ZrO_2 in water, 0.1 μm particle size, supplied by Alfa Aesar). Inductively coupled plasma-optical emission spectroscopy (ICP-OES) analysis revealed a content of 1.09% of Hf and 168 ppm of iron. Before use the zirconia was calcined and sintered in air at various temperatures, leading to a systematically controlled surface area.[34] The surface area of the samples was determined by adsorption of nitrogen at 77 K according to BET (Fig. 1). The structure of the samples during thermal and vacuum treatment was investigated by X-ray diffraction (XRD) and Raman spectroscopy.

The nanocrystalline "fresh" sample (n-ZrO_2) crystallizes in the monoclinic structure with an average crystallite size of 5 nm, as revealed by X-ray line broadening. It has a BET surface area of 115–120 $m^2\ g^{-1}$ and is thermally stable up to 723 K, above which the zirconia starts to sinter. Upon sintering the specific surface area decreases continuously with increasing calcination temperature leading to a value of 13 $m^2\ g^{-1}$ after calcination at 1273 K (Fig. 1). This latter sample still exhibits the monoclinic structure with a crystallite size of 20 nm. Thus, the subsequent data were obtained with two different zirconia samples: the nanocrystalline sample (calcined at 673 K), which was only used at temperatures below 723 K to avoid sintering, and the fully sintered sample (calcined at 1273 K).

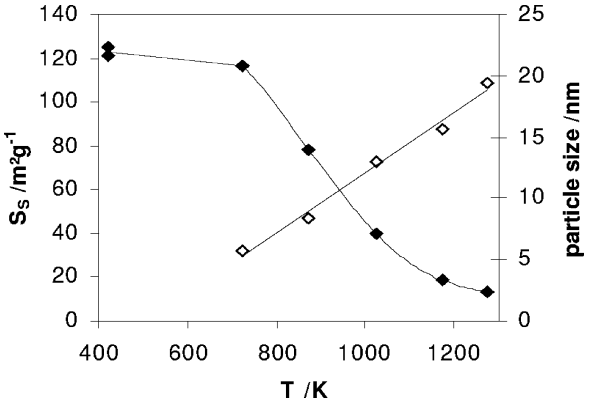

Fig. 1 BET surface area of zirconia calcined at various temperatures (•) and corresponding size of crystallites deduced from X-ray line width broadening (◇).

Hydrogen, helium and oxygen were highest grade gases supplied by Messer–Griesheim. Hydrogen was further purified by passing through an oxygen removing purifier, and helium was freed from traces of oxygen with an Anoxy-Cil unit. Condensable contaminants were removed from hydrogen and helium by liquid nitrogen traps, while oxygen was passed through a trap cooled with liquid nitrogen–ethanol.

Volumetric apparatus

Volumetric measurements were performed in an all glass apparatus as described previously.[34] Zirconia was treated in flowing dry hydrogen at a typical flow rate of 1 ml s^{-1}. In order to control the activity of oxygen, in some experiments the hydrogen was passed through an U-shaped tube whose bottom was covered by H_2O. Upon cooling to 273 K, the vapour pressure of water in the resulting gas stream was fixed at 6.1 mbar.

Electrochemical impedance spectroscopy

An IM6e impedance spectrometer (Zahner-Elektrik) was used to measure the magnitude of the impedance and the phase shift between current and voltage (50 mV a.c.) in a frequency range of 10 mHz to 1 MHz. The impedance spectra were acquired using the 2-pole mode with gold electrodes, as described elsewhere.[47]

To retain ready gas access to the zirconia surface, the samples were compressed with low pressure (2000 bar) to produce pellets of about 1 mm thickness and 6 mm diameter. To minimize the contact resistance, thin layers of gold were deposited on both sides of the pellets by high vacuum deposition. The pellets were placed in a quartz glass tube equipped with gold electrodes that were pressed onto the pellet with 1 bar. The apparatus is suitable for different gas treatments

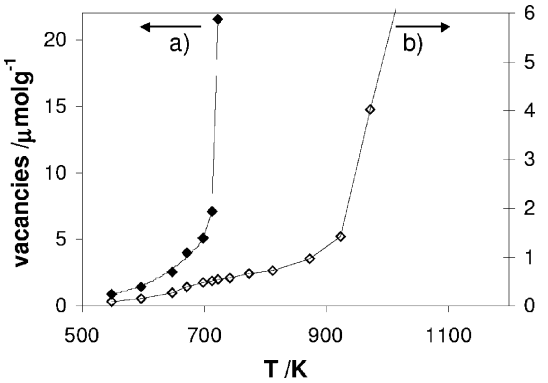

Fig. 2 Number of vacancies in nanocrystalline ZrO_2 (a) and sintered ZrO_2 (b) after reduction for two hours at various temperatures.

and is described elsewhere.[36] Some measurements were performed with a water vapour pressure of 6.1 mbar by passing the gases through a trap in which water was held at 273 K. Samples were heated up to 1073 K with a tubular oven that was controlled by a Ni/NiCr thermocouple, situated in the reactor about 5 mm downstream of the pellet.

Results

Effect of surface area on the number of oxygen vacancies

In a previous paper we discussed the formation of oxygen vacancies in ZrO_2 and the effect of various parameters including reduction temperature, reduction time, and water vapour pressure.[34] These studies were done on fully sintered zirconia samples that had been prepared by calcination in air at 1273 K. In contrast, the present work considers the fresh, nanocrystalline ZrO_2 samples (n-ZrO_2) that had been treated in hydrogen containing 6.1 mbar water vapour at temperatures below 723 K.

Fig. 2 shows the increase in the number of oxygen vacancies as obtained by volumetric oxygen titration with increasing reduction temperature for both the nanocrystalline zirconia (a) and the sintered sample (b). Both samples exhibit a similar behaviour when reduced at temperatures below 673 K. Assuming a partial equilibrium between the gas phase and the surface of zirconia, the van't Hoff plot revealed an energy of 25 kJ mol^{-1} (0.26 eV) for both samples, which is assumed to be the energy needed for the formation of oxygen vacancies on the surface of ZrO_2.[34]

The number of oxygen vacancies on a per-weight basis is higher in the nanocrystalline sample by a factor of about 10. We point out that this is also the ratio of the specific surface areas between the nanocrystalline ($\sim$120 m^2 g^{-1}) and sintered sample ($\sim$13 m^2 g^{-1}) as shown in Fig. 1. Thus, relative to the surface area, the concentration of the oxygen vacancies is the same in both samples. This direct relationship between the number of vacancies and the surface area supports our assumption that at least in the given temperature range the oxygen vacancies are concentrated at the surface.

When the reduction temperature is raised above 673 K, the increase in the number of vacancies is significantly different for the two samples. While the number of oxygen vacancies in the nanocrystalline sample continues to increase rapidly with increasing reduction temperature, the formation of oxygen vacancies in the latter seems to be hindered and temperatures above 873 K are needed for a further increase. The activation energy needed for the formation of these vacancies was calculated to be 115 kJ mol^{-1} (1.2 eV) as obtained from the Arrhenius plots. The relevant processes described by this activation energy include the formation of surface vacancies and their diffusion through the bulk. Thus, the vacancies in nanocrystalline zirconia seem to diffuse from the surface into the bulk at much lower temperatures (673 K) than in sintered zirconia (873 K).

Impedance spectroscopy of zirconia in oxygen

(a) Nanocrystalline zirconia. Pure zirconia is an insulator at room temperature with capacitive behaviour in the whole frequency range. With increasing temperature zirconia becomes a semiconductor, exhibiting capacitive conduction at high frequencies and a parallel ohmic conduction in the low frequency range (Fig. 3a). The corresponding phase shift changes from -90° in the high frequency region (capacitive) to 0° in the low frequency region (ohmic). With increasing temperature the low frequency resistance decreases from about 2 GΩ at 623 K to about 150 MΩ at 723 K. This behaviour is typical for semiconducting materials.[51]

Beyond 0.1 Hz an additional impedance contribution is observed which increases with decreasing frequency. In this frequency range the phase shifts to negative values again (Fig. 3a). This indicates that an additional capacitive impedance contributes to the total impedance even at this low frequency. The height of the impedance step in this frequency range increases with increasing temperature. We found a similar behaviour for nanocrystalline titania, for which we proposed a mechanism including a parallel pathway.[42]

(b) Sintered zirconia. For comparison, samples of sintered zirconia were treated in flowing oxygen at various temperatures. Fig. 3b shows the corresponding impedance spectra taken at 723 K. The impedance at high frequencies for the sintered sample is similar to that of the nanocrystalline sample; however, it is significantly different at low frequencies, with

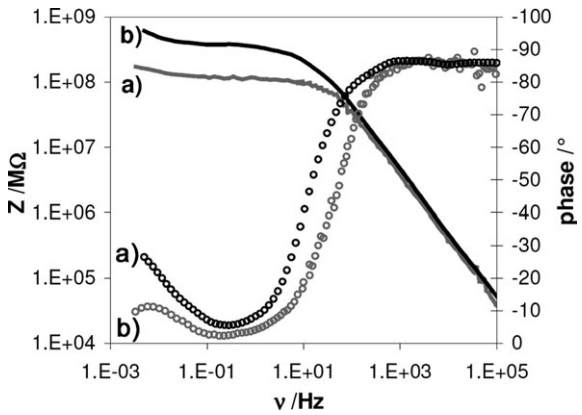

Fig. 3 Bode plot with impedance (—) and phase shift (○) for (a) nanocrystalline ZrO_2 and (b) sintered ZrO_2 in dry oxygen at 723 K.

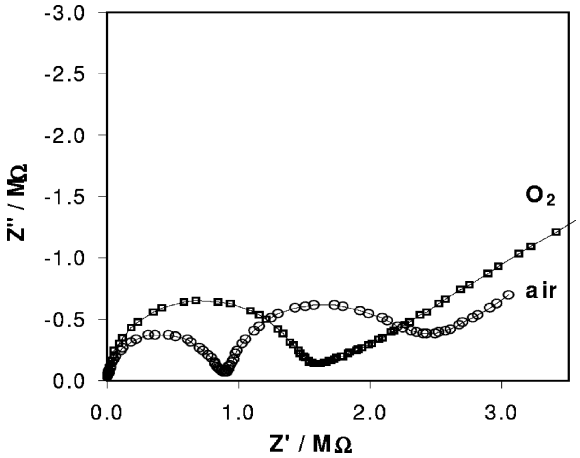

Fig. 4 Nyquist plot of nanocrystalline ZrO_2 treated in dry oxygen (▭) and in ambient air (○) at 1073 K.

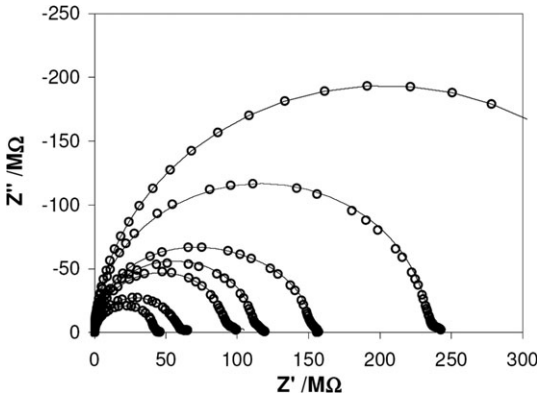

Fig. 5 Nyquist plots (○) of nanocrystalline ZrO_2 obtained after treatment in wet hydrogen at temperatures between 523 K and 713 K (25° steps) and curves (—) simulated with proposed equivalent circuit model.

higher values in the sintered sample. Below 0.1 Hz the impedance increases again and the phase shift to negative values is even more pronounced and now seems to reach −45°, which is typical for diffusion controlled conduction processes.[51]

Effect of gas treatments

(a) Treatment in oxygen and in ambient air. To study the effect of oxygen partial pressure the nanocrystalline zirconia sample was treated in flowing dry oxygen as well as in ambient air. The Nyquist spectrum for zirconia in flowing dry oxygen in Fig. 4b was measured at 1073 K and shows a slightly depressed semicircle in the high frequency region, similar to the spectrum of nanocrystalline zirconia at lower temperatures. The time constant for this process was calculated from the impedance data to be 76 μs. At low frequencies, a linear increase with a 45° slope indicates a diffusion-limited process, which is also present (but less evident) at lower temperatures.

When zirconia is treated in ambient air an additional semicircle appears, leading to a higher overall impedance compared to the oxygen treated sample (Fig. 4a). The first semi-circle at high frequencies is almost not suppressed and corresponds to a process with a time constant of 40 μs. In both samples, this rather fast process is probably due to electronic transport.[51] The well separated second semi-circle describes a much slower process with a time constant of 0.2 s.

(b) Treatment in hydrogen. The impedance of zirconia treated in hydrogen containing 6.1 mbar water at room temperature is similar to the corresponding value of oxygen treated zirconia, even after long treatments. With increasing reduction temperature, the low frequency impedance of hydrogen treated zirconia decreases with increasing reduction temperature from 240 MΩ at 573 K to 45 MΩ at 713 K. We found that sintering of zirconia occurred at lower temperatures when exposed to hydrogen than to oxygen (713 K *vs.* >723 K). Thus, the reduction temperature for the nanocrystalline sample was always kept below 713 K to avoid further sintering.[34] The corresponding Nyquist spectra consists of only one, slightly suppressed semicircle (Fig. 5) and no signs of a second conduction pathway in the low frequency region were found.

Discussion

Mechanism of conduction

Zirconia doped by low-valent cations like Y^{3+} or Ca^{2+} are prime examples of ionic conductors. In pure zirconia a residual number of anion vacancies remains due to contaminants in the material and thermodynamic disorder equilibrium, but electronic conduction may also contribute to the observed finite conductivity.

Thus, we applied an equivalent circuit model, combining both ionic and electronic conduction, that was recently developed for titania.[47] Considering all contributions to the overall impedance, we propose the following scheme for the conduction mechanism, occurring (i) *via* pathway A by electronic conduction and (ii) *via* pathway B by ionic transport. The serial contributions of pathway A describe the electron transport from the electrode to the oxide (ct), electronic conduction through the oxide (b), and electron transport between the oxide grains (gb) and are each characterised by an ohmic resistor in parallel to a capacitor.

In pathway B the ionic conduction is characterised by an ohmic resistor (R_i). Since the ionic motion may be impeded by diffusion limitations, especially at low frequencies, a simple distributive impedance element, the Warburg impedance element (W), was added to the circuit diagram. At the limit of low frequencies the impedance of pathway B increases and the phase shift changes to negative values. The reason for this breakdown of the surface conduction may arise from ion blocking by grain boundaries perpendicular to the charge flow, or by ion blocking at the interface to the gold electrode. In both cases this blocking is characterised by a capacitor (C_e) in series to the resistor R_i. The resulting equivalent circuit diagram is shown in Fig. 6.

In order to prove the validity of the proposed mechanism we compared the experimentally obtained impedance spectra (data points), depicted as Nyquist diagrams, with the impedance simulated from the circuit diagram (continuous line).

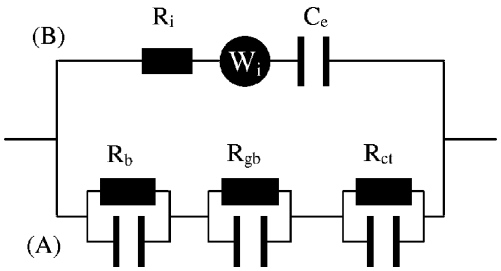

Fig. 6 Circuit diagram equivalent to the conduction mechanism, subscripts of the RC combinations are: b for bulk, gb for grain boundary, ct for charge transfer at the electrode, R_i and W_i denote the ionic resistance and Warburg impedance, C_e the ionic capacitance at the electrodes.

For some data the omission of any impedance element from the equivalent circuit may give sufficient agreement, but all elements of this circuit are necessary to describe all results obtained in this work. The agreement of the simulated spectra with the experimental data supports the validity of the circuit diagram. One could envision other equivalent circuit models that would fit the data reasonably well; however, the chosen model was most appropriate to the present physical chemical data. The simulation of the experimental data and their fitting to obtain optimum parameters further allows us to calculate the individual impedance contributions.

Oxygen treated samples

Effect of surface area. Fig. 7 shows the experimental Nyquist spectra (data points) and the data calculated with the proposed equivalent circuit (continuous line) for both the high-surface sample (a) and the low-surface sample (b) treated in dry oxygen at 723 K. The fitted parameters of the equivalent circuit (normalised to the surface of the electrodes and the thickness of the pellets) are given in Table 1.

The bulk resistance for the sintered zirconia (R_b) is about 60% higher than that of fresh zirconia. Hence, the high surface sample ($d \approx 5$ nm) exhibits a significantly higher electronic conductivity than the low surface sample ($d \approx 20$ nm). In the case of electronic conduction through the bulk the conductivity is not expected to depend on the particle size, in contrast to a conduction on the surface. This suggests that part of the

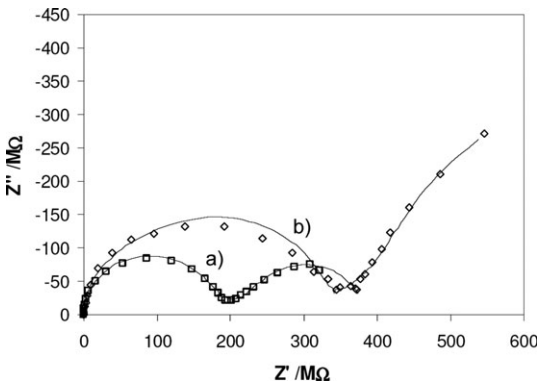

Fig. 7 Nyquist plot of nanocrystalline ZrO_2 (a) and sintered ZrO_2 (b) in dry oxygen at 723 K: experimentally obtained data (□ and ◇) and simulated curve by proposed equivalent circuit model (—).

Table 1 Calculated equivalent data of nanocrystalline (fresh) and sintered ZrO_2 treated in oxygen at 723 K

	Fresh	Sintered
R_b/MΩ	238	398
C_b/pF	62.3	60.8
R_{gb}/MΩ	14.5	70.5
C_{gb}/pF	4210	74
R_{ct}/MΩ	134.8	619
C_{ct}/nF	124	90
R_i/MΩ	563	1037
W_i/MΩ $s^{-1/2}$	540	566
C_i/nF	145	7.1

conductivity in the high surface material occurs near the surface area of zirconia. Additionally, the proportional effect of the surface area on the number of oxygen vacancies indicates that the electrons introduced during the reduction are located near the surface of zirconia. Thus, we assume that part of the electronic conduction occurs near the surface of the zirconia particles.

The obtained bulk capacity (C_b) values were similar for both the fresh and sintered samples. Below 723 K these values were independent of the temperature. The corresponding dielectric constants (between 12 and 13), calculated from this bulk capacitance, agree well with literature data for monoclinic zirconia (12.4 [51]) and therefore support the proposed model.

The contribution of the grain boundaries to the overall electronic impedance leads to a considerably higher capacitance (C_{gb}) for the high surface sample due to the larger number of grain boundaries to be passed. On the other hand, the ohmic grain boundary resistance (R_{gb}) of the high surface sample is lower than that of the low surface sample. This apparent discrepancy can be resolved by recognising that during sintering the volume of the particles probably shrinks, leading to an increased mean distance between the grains. As a result, the charge transport between the grains is inhibited, thereby causing a higher overall ohmic resistance, despite the lower number of passages between grain boundaries for the sintered sample.

The resistance of the ionic pathway (R_i) is also lower for the high surface sample, providing further evidence that the ionic conduction is confined to the surface. The high capacitance that blocks the ionic pathway suggests that the transfer and therefore the discharge of ions at the electrodes is inhibited, presumably due to the low exchange current density of oxygen at the gold electrode.

Effect of the oxygen partial pressure. The ohmic resistance of the air treated sample (at 1073 K) is higher by a factor of about 1.7 compared to the treatment in pure hydrogen (Fig. 4). This result indicates that at least at those high temperatures charge carriers may be formed during the reduction of Zr^{4+} *via* the equation:

$$Zr^{4+} + O^{2-} + \rightarrow V_O + e^- + Zr^{3+} + 1/2O_2 \qquad (1)$$

In equilibrium reactions the surface oxygen vacancies and the Zr^{3+} ions may also form a surface complex, following

$$Zr^{3+} + V_O \rightarrow + Zr^{3+}\text{–}V_O \qquad (2)$$

Furthermore, one has to consider that the electrons may be captured by an oxygen vacancy or by an Zr^{3+} –V_O complex to form surface F centers, with the electrons presumably occupying donor sites in the bulk of the zirconia.

The number of defects, which are formed independently due to the release of an oxygen atom, can be estimated by the effect of oxygen pressure on the impedance. This is assuming that the electronic conduction at any given temperature is proportional to the number of electrons formed and independent of whether they are bound to oxygen vacancies or to donor sites. The law of mass action then gives the equation $K = {p_{O_2}}^{1/2} x^n$, where x is the concentration of the electrons and n is the number of independently formed defects. According to this relation the electronic conductivity, and hence the number of electrons, should be proportional to ${p_{O_2}}^{-1/2n}$. In this work we found that the conductivity of zirconia is higher by a factor of 1.7 when treated in air compared to pure oxygen. Consequently, this ratio suggests that for each oxygen atom released 1.5 defects are formed independently. Thus, we have to assume that Zr^{3+} and oxygen vacancies indeed form a surface complex and that approximately half of the electrons are bound to that complex while the other half of the electrons occupy independent sites.

Hydrogen treated samples

When zirconia was treated in hydrogen the low frequency impedance of both samples decreased by a factor of 3–4 (Fig. 8 and 9). This effect is much smaller in zirconia than in titania,[52] where the conductance between the hydrogen and oxygen treated samples differs by a factor as high as 10^6. Nevertheless the mechanism for this hydrogen effect may be the same as in titania, according to the equation

$$O^{2-}{}_s + H_{2,g} \Leftrightarrow V_s + 2e^- + H_2O_g \qquad (3)$$

The extent of reduction, however, is much smaller in zirconia and the electrons are probably confined to the surface (V_s). According to this equation, the vapour pressure of water significantly affects the equilibrium of the reaction and thus was maintained at 6.1 mbar (water vapour pressure at 0 °C).

The experimental data (data points) agree very well with the simulated impedance values upon applying the proposed equivalent circuit (continuous line). Due to the enhanced

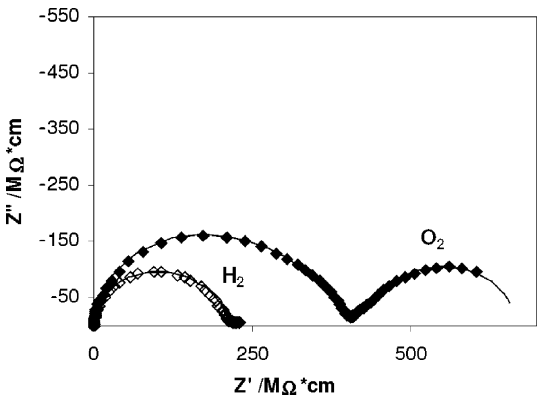

Fig. 8 Nyquist plot of nanocrystalline ZrO_2 at 713 K in hydrogen and oxygen.

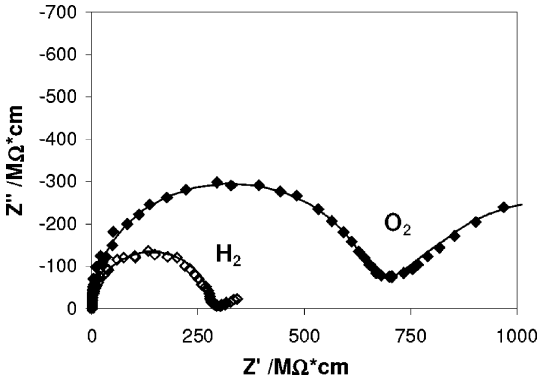

Fig. 9 Nyquist plot of sintered ZrO_2 at 713 K in hydrogen and oxygen.

electronic conduction the ionic contribution now becomes negligible resulting in scattered parameters for ionic conduction in the data fit. Thus, for the analysis of the hydrogen data, the pathway B in the equivalent circuit was omitted.

Table 2 shows the fitting parameters for the electronic conduction obtained for different temperatures. The bulk capacitance slightly increases with increasing temperature, and the calculated values for the dielectric constant (11–13) are similar to those of zirconia treated in oxygen.

Generally, the ohmic resistances decrease with increasing temperature indicating activated processes. An Arrhenius analysis of the overall conductivity data taken at 1.3 Hz (Fig. 10) reveals two regimes characterised by different activation energies. Below 673 K, the sum of all resistive contributions results in an apparent activation energy of 25 kJ mol^{-1} (0.26 eV). Above 673 K the electronic conduction along the surface is characterised by an apparent activation energy of 100 kJ mol^{-1} (1.04 eV), the energy barrier for electronic conduction across the grain boundaries is 125 kJ mol^{-1} (1.3 eV) and the transfer of electrons to the gold electrode needs 65 kJ mol^{-1} (0.67 eV). Therefore, we conclude that the electronic transport along the zirconia surface is again the main contribution to the ohmic resistance in pathway A.

Energy level of the donor sites

The apparent activation energy for electronic conduction arises from the effect of temperature on the number of charge carriers as well as the energy needed to enable the promotion of electrons from the donor sites to the conduction band.

Table 2 Calculated equivalent data (only path A) of nanocrystalline ZrO_2 treated in hydrogen containing 6.1 mbar water at various temperatures

T/K	R_b/MΩ	C_b/pF	R_{gb}/MΩ	C_{gb}/pF	R_{ct}/MΩ	C_{ct}/nF	R_{ges}/MΩ
523	322	3.4	78	214	8.0	910	408,0
573	196	3.5	42	220	7.0	950	245,0
623	124	3.8	28	216	4.3	916	156,3
653	99	4.5	20	216	3.2	916	122,2
673	89	4.1	18	214	2.7	740	109,9
693	52	4.3	9	212	1.9	568	63,1
713	34	4.7	5	216	1.4	206	40,5

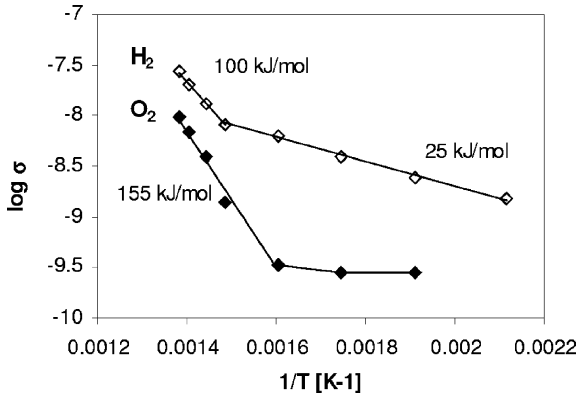

Fig. 10 Arrhenius plot of conductivity measured at 1.3 Hz *versus* temperature for nanocrystalline ZrO_2 treated in oxygen and in hydrogen.

Hydrogen treatment leads to an oxygen surface vacancy along with two free electrons (eqn (3)), or one free electron and a Zr^{3+} ion, if some fractions of these electrons are localised at the zirconium ions. The energy needed for this process is 25 kJ mol^{-1} (0.26 eV) when reduction was carried out at temperatures below 873 K.[34] For this temperature range it could be shown that oxygen vacancies are formed at the surface of the oxide, and that their number is directly proportional to the specific surface area. As a result, both electrons and vacancies are confined to the surface. The energy needed for the formation of these electrons is 25 kJ mol^{-1} of 0.27 eV.

The apparent activation energy for electronic conduction after treatment in hydrogen in the temperature range between 673 K and 873 K is 1.04 eV. After subtracting the energy needed for the formation of electrons (0.26 eV), the remaining apparent activation energy (0.78 eV) is consistent with the energy needed to promote the electrons from their intergap sites to the conduction band. This result is in reasonable agreement with recent calculations by Shluger *et al.*, who proposed that the formation of F^{2+} centres in hydrogen treated monoclinic zirconia occurs at 1 eV below the conduction band.[27] This suggests that further to the oxygen vacancies the electrons are also localised at the surface or grain boundaries, as proposed from the proportionality between oxygen vacancies and specific surface area. Furthermore, these results support the assumption that the electrons move along the surface rather than through the bulk of the grains.

However, a different situation is found at temperatures below 653 K, where the activation energy for bulk conduction in the oxygen treated low-surface sample is 0.26 eV, indicating a different conduction mechanism. Most likely, extrinsic dopants like iron ions form charge carriers, their number being independent of temperature. The measured apparent activation energy for electronic conduction is therefore expected to be equal to the energy needed for activation alone. If that is the case these electrons would occupy donor sites 0.26 eV below the conduction band.

For comparison, zirconia treated in oxygen exhibits a stronger temperature dependence with an activation energy of 150 kJ mol^{-1} (1.55 eV). The activation energy for oxygen diffusion is generally greater than 200 kJ mol^{-1} (2 eV),[39] which seems to exclude this mechanism of conduction. However, it could be shown that doping of zirconia with Ca^{2+} or Y^{3+} ions, typically used in SOFC, reduces the energy needed for oxygen diffusion to approximately 120 kJ mol^{-1} (1.24 eV).[53] In this sample, the iron content may reduce the activation energy in a similar way.

Conclusions

The partial reduction of monoclinic zirconia (ZrO_2) in hydrogen and its effect on the electric performance was investigated using volumetric oxygen titration, temperature programmed oxidation/desorption and electrochemical impedance spectroscopy. Hydrogen treatment below 873 K leads to the formation of oxygen vacancies at the surface (apparent activation energy $\sim$25 kJ mol^{-1}), while at higher temperatures the vacancies were able to diffuse into the bulk ($\sim$115 kJ mol^{-1}). The formation of these vacancies is accompanied by the release of electrons, their number being directly proportional to the specific surface area. These electrons were found to be confined to the surface and need 0.78 eV to be raised to the conduction band.

References

1 N. Stetter and R. Waser, *Acta Mater.*, 2000, **48**, 151.
2 C. J. Kevane, *Phys. Rev.*, 1964, **133**(5A), 1431–1436.
3 A. K. Jonsson, G. A. Niklasson and M. Veszelei, *Thin Solid Films*, 2002, **402**, 242–247.
4 R. Ramamoorthy, D. Sundararaman and S. Ramasamy, *Solid State Ionics*, 1999, **123**, 271–278.
5 H. L. Tuller, *Solid State Ionics*, 2000, **131**, 143–157.
6 J.-H. Lee, *J. Mater. Sci.*, 2003, **38**, 4247–4257.
7 A. D. Brailsford, M. Yussouff and E. G. Logothetis, *Sens. Actuators, B*, 1997, **44**, 321–326.
8 G.-L. Tan and X.-J. Wu, *Thin Solid Films*, 1998, **330**, 59–61.
9 K. R. Sridhar and J. A. Blanchard, *Sens. Actuators, B*, 1999, **59**, 60–67.
10 N. Q. Minh, *J. Am. Ceram. Soc.*, 1993, **76**(3), 563–588.
11 S. P. Jiang and S. P. S. Badwal, *Solid State Ionics*, 1999, **123**, 209–224.
12 M. S. Isaacs, in *Science and Technology of Zirconia, Advances in Ceramics*, ed. A. H. Heuer and L. W. Hobbs, American Ceramics Society, Columbus, OH, 1981, vol. 3, p. 406.
13 T. Yamaguchi, *Catal. Today*, 1994, **20**, 199–218.
14 A. Methivier and M. Pijolat, *J. Catal.*, 1993, **139**(2), 329–337.
15 G. Centi, B. Panzacchi, S. Perathoner and F. Pinna, *Stud. Surf. Sci. Catal.*, 2000, **130**, 2273–2278.
16 V. Indovina, *Catal. Today*, 1998, **41**, 95–109.
17 N. Yamamotoa, S. Sato, R. Takahashi and K. Inui, *J. Mol. Catal. A: Chem.*, 2006, **243**, 52–59.
18 F. Audry, P. E. Hoggan, J. Saussey, J. C. Lavalley, H. Lauron-Pernot and A. M. L. Govic, *J. Catal.*, 1997, **168**, 471–481.
19 K. Tanabe and T. Yamaguchi, *Catal. Today*, 1994, **20**, 185–198.
20 B. C. Klose, F. C. Jentoft, R. Schloegl, I. R. Subbotina and V. B. Kazansky, *Langmuir*, 2005, **21**(23), 10564–10572.
21 E. Mamontov, T. Egami, R. Brezny, M. Koranne and S. Tyagi, *J. Phys. Chem. B*, 2000, **104**, 11110–11116.
22 F. Fally, V. Perrichon, H. Vidal, J. Kaspar, G. Blanco, J. M. Pintado, S. Bernal, G. Colon, M. Daturi and J. C. Lavalley, *Catal. Today*, 2000, **59**, 373–386.
23 E. Ryshkewitch and D. W. Richerson, *Oxide Ceramics*, Academic Press, Orlando FL, 1985.
24 K. H. Jacob, E. Knözinger and S. Benfer, *J. Chem. Soc., Faraday Trans.*, 1994, **90**(19), 2969–2975.
25 A. Christensen and E. A. Carter, *Phys. Rev. B*, 1998, **58**, 8050–8064.
26 S. Fabris, A. T. Paxton and M. W. Finnis, *Phys. Rev. B*, 2000, **61**(10), 6617–6629.

27 A. S. Foster, V. B. Sulimov, F. L. Gejo, A. L. Shluger and R. M. Nieminen, *Phys. Rev. B*, 2001, **64**, 224108.
28 S. Gennard, F. Cora and C. R. A. Catlow, *J. Phys. Chem. B*, 1999, **103**, 10158–10170.
29 A. Eichler and G. Kresse, *Phys. Rev. B*, 2004, **69**(4), 045402.
30 A. Hofmann, S. J. Clark, M. Oppel and I. Hahndorf, *Phys. Chem. Chem. Phys.*, 2002, **4**(14), 3500–3508.
31 M. Daturi, C. Binet, S. Bernal, J. A. P. Omil and J. C. Lavalley, *J. Chem. Soc., Faraday Trans.*, 1998, **94**(8), 1143–1147.
32 C. Morterra, E. Giamello, L. Orio and M. Volante, *J. Phys. Chem.*, 1990, **94**, 3111–3116.
33 M. Maczka, E. T. G. Lutz, H. J. Verbeek, K. Oksam, A. Meijerink, J. Hanuza and M. Stuivinga, *J. Phys. Chem. Solids*, 1999, **60**, 1909–1914.
34 D. Eder and R. Kramer, *Phys. Chem. Chem. Phys.*, 2002, **4**(5), 795–801.
35 A. Trunschke, D. L. Hoang and H. Lieske, *J. Chem. Soc., Faraday Trans.*, 1995, **91**(24), 4441–4444.
36 D. Eder and R. Kramer, *Phys. Chem. Chem. Phys.*, 2003, **5**(6), 1314–1319.
37 H. Haerudin, S. Bertel and R. Kramer, *J. Chem. Soc., Faraday Trans.*, 1998, **94**, 1481–1487.
38 U. Brossmann, G. Knöner, H.-E. Schäfer and R. Würschum, *Rev. Adv. Mater. Sci.*, 2004, **6**, 7–11.
39 U. Brossmann, U. Södervall and H.-E. Schäfer, *J. Appl. Phys.*, 1999, **85**(11), 7646–7654.
40 I. Kosacki, T. Suzuki, V. Petrovsky and H. U. Anderson, *Solid State Ionics*, 2000, **163–137**, 1225–1233.
41 P. Knauth and H. L. Tuller, *Solid State Ionics*, 2000, **136–137**, 1215–1224.
42 A. Tschöpe, J. Y. Ying and H. Tuller, *Sens. Actuators, B*, 1996, **31**, 111–114.
43 S. Bhowmik, K. P. Constant, J. C. Parker and M. Ali, *Mater. Sci. Eng., A*, 1995, **204**, 258–266.
44 K. H. Kim, E. J. Oh and J. S. Choi, *J. Phys. Chem. Solids*, 1984, **45**((11/12)), 1265–1269.
45 H. Näfe, *Solid State ionics*, 1984, **13**, 255–263.
46 M. Levy, J. Fouletier and M. Kleitz, *J. Electrochem. Soc.*, 1988, **135**(6), 1584–1589.
47 D. Eder and R. Kramer, *J. Phys. Chem. B*, 2004, **108**(39), 14823–14829.
48 I. Kosacki, B. Gorman and H. U. Anderson, in *Ionic and Mixed Conductors*, ed. T. A. Ramanarayanam, The Electrochemical Society, Pennington, NJ, 1998, vol III, p. 631.
49 W. Göpel and G. Reinhardt, *Metal Oxide Sensors: New Devices Through Tailoring Interfaces on the Atomic Scale*, in *Sensors Update Sensor Technology-Applications-Market*, ed. H. Baltes, W. Göpel and J. Hesse, VCH, Weinheim, 1996, p. 49.
50 C. A. J. Fisher and H. Matsubara, *Solid State Ionics*, 1998, **113–115**, 311–318.
51 *Impedance Spectroscopy Emphasizing Solid Materials and Systems*, ed. J. R. Macdonald, John Wiley and Sons, 1987.
52 H. Haerudin, S. Bertel and R. Kramer, *J. Chem. Soc., Faraday Trans.*, 1998, **94**, 1481–1487.
53 L. A. Simpson and R. E. Carter, *J. Am. Ceram. Soc.*, 1966, **49**, 139.